NMR study of local structure and chemical ordering in $PbMg_{1/3}Nb_{2/3}O_3$ and $PbSc_{1/2}Nb_{1/2}O_3$ relaxor ferroelectrics

V. V. Laguta,[1] M. D. Glinchuk,[1] S. N. Nokhrin,[1] I. P. Bykov,[1] R. Blinc,[2] A. Gregorovič,[2] and B. Zalar[2]
[1]*Institute for Problems of Material Sciences, Ukrainian Academy of Sciences, Krjijanovskogo 3, 03142 Kiev, Ukraine*
[2]*Jožef Stefan Institute, Jamova 39, 1000 Ljubljana, Slovenia*

(Received 11 September 2002; revised manuscript received 22 November 2002; published 25 March 2003)

The ^{93}Nb and ^{45}Sc nuclear-magnetic-resonance (NMR) spectra of disordered relaxor ferroelectrics $PbSc_{1/2}Nb_{1/2}O_3$ (PSN) and $PbMg_{1/3}Nb_{2/3}O_3$ (PMN) have been studied at $T>T_m$, where $T_m \approx 355$ K and 265 K is the temperature of the dielectric susceptibility maximum for PSN and PMN, respectively. The analysis of the spectra was performed both on the basis of an analytical description of the NMR line shapes, allowing for homogeneous and inhomogeneous broadening related to a random distribution of the electric-field gradients, and a numerical Monte Carlo approach taking into account electric-field gradients originating from the random distribution of Mg, Sc, and Nb ions (which may be shifted or not) over *B*-type cation sites. $1/2 \leftrightarrow -1/2$ NMR spectra of ^{93}Nb and ^{45}Sc in PSN contain a narrow (3–4 kHz) almost isotropic component and a broad strongly anisotropic component. These two components of the NMR spectra are related to the 1:1 Sc/Nb ordered and compositionally disordered regions of the crystal, respectively. It is shown that in the disordered regions, the Sc^{3+}, Nb^{5+}, and O^{2-} ions are randomly shifted from their cubic lattice sites in one of the three possible directions: $\langle 100\rangle$, $\langle 110\rangle$, or $\langle 111\rangle$. In PMN, the NMR spectrum of ^{93}Nb contains practically only the broad component. The portion of the unbroadened spectrum that may correspond to ideal 1:2 Mg/Nb ordered regions accounts only for 2–3 % of the total integral intensity. No evidence was obtained for the existence of 1:1 Mg/Nb regions in PMN. The NMR data demonstrate that in PMN the cubic symmetry at $T>T_m$ is locally broken due to ion shifts similar to that in disordered PSN. The values of the ionic shifts have been estimated in the point-charge point-dipole approximation for the electric-field gradients both in PSN and PMN.

DOI: 10.1103/PhysRevB.67.104106 PACS number(s): 77.84.Dy, 76.30.Fc

I. INTRODUCTION

Relaxor ferroelectrics[1,2] have attracted considerable attention in recent years due to their unusual physical behavior. Lead magnesium niobate, $PbMg_{1/3}Nb_{2/3}O_3$ (PMN), is probably the best investigated relaxor crystal. It displays high dielectric permittivity over a broad temperature range with a significant frequency dispersion ($\varepsilon' \simeq 20\,000$ at $T_m = 265$ K and $f = 1$ kHz) and giant electrostriction.[2] Contrary to normal ferroelectrics, such anomalies are not directly linked to a structural phase transition but related to relaxational processes. Indeed in PMN, x-ray and neutron-diffraction studies showed no evidence for a structural phase transition down to 5 K; the symmetry remains cubic on an average, whatever the temperature,[3] contrary to the $PbSc_{1/2}Nb_{1/2}O_3$ (PSN) relaxor, which undergoes a spontaneous cubic-rhombohedral phase transition at $T_m \simeq 355$ K.[4] However, this is only an average situation. Structural refinement results have shown that the local structure is different from the average cubic one for both of the relaxors, and even at $T \gg T_m$.[4,5] For instance, Pb^{2+} ions are randomly shifted below ≈ 650 K,[6] i.e., far above T_m. At this high temperature, the optic index of refraction $n(T)$ deviates from a linear temperature dependence as it was first evidenced by Burns and Dacol.[7] They assumed that this unexpected high-temperature deviation arises from small, randomly oriented, very local regions of nonreversible polarization that begin to appear within the otherwise nonpolar crystal structure below T_d, which is called the Burns temperature. The formation of polar nanoregions was also confirmed by observation in the PMN x-ray and neutron diffuse scattering that appears below T_d.[3,8] Recent neutron inelastic-scattering measurements demonstrate that polar nanoregions are related to condensation of the lowest-energy transverse-optic (TO) phonon mode at T_d.[9,10]

A number of important questions, however, still remain open. The first is which ion displacements (Pb or Nb/Mg/Sc) are responsible for the formation of polar regions? What is the nature of nonpolar matrix into which polar clusters are assumed to be embedded? Are the polar clusters and the nonpolar matrix dynamic or static entities? Another still open important problem in PMN relaxor is related to microscopic inhomogeneities in the site occupancy of the Mg^{2+} and Nb^{5+} cations and their role in the formation of the polar regions. An existence of a 1:1 Mg/Nb ordered microregions is still discussed in literature (see, for example, Refs. 11 and 12). Since the 1:1 Sc/Nb chemical order in $PbSc_{1/2}Nb_{1/2}O_3$ really exists, a comparative study of the high-temperature local structure of these two relaxors is of interest.

It should be stressed that the diffraction methods do not provide complete characterization of lattice distortions and ionic shifts in relaxors due to the compositional disorder of these materials and nanometric scale of polar order. Thus, local methods such as magnetic resonance and, in particular, nuclear magnetic resonance (NMR) can be extremely useful in this case. In NMR experiments, the nuclei are sensitive to their local environment at a distance less than 1–2 nm. In addition, NMR operates at a much longer time scale (10^{-5}–10^{-8} s) in comparison with the neutron or x-ray methods that also provide the possibility to distinguish be-

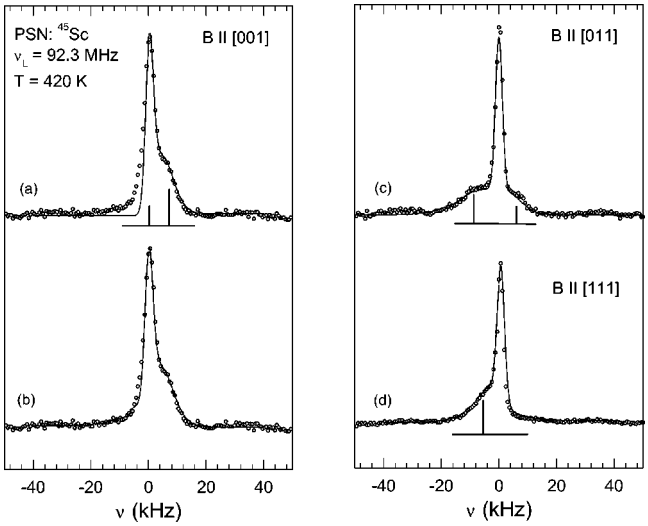

FIG. 1. ^{45}Sc NMR spectra in PSN. Points are experimental data; smooth lines correspond to calculated according to Eqs. (6)–(8) line shapes for (a) and (b) $\mathbf{B}\|[001]$, (c) $\mathbf{B}\|[011]$, (d) $\mathbf{B}\|[111]$. The diagrams schematically show expected NMR resonances for second-order quadrupole contribution with the EFG axis pointed along $\langle 001\rangle$ directions. Calculated line shapes include contributions from ideal cubic regions plus axial EFG pointed at (a) $\langle 001\rangle$ directions; (b), (c), and (d) $\langle 001\rangle$, $\langle 011\rangle$, and $\langle 111\rangle$ directions in proportions given by Eq. (8).

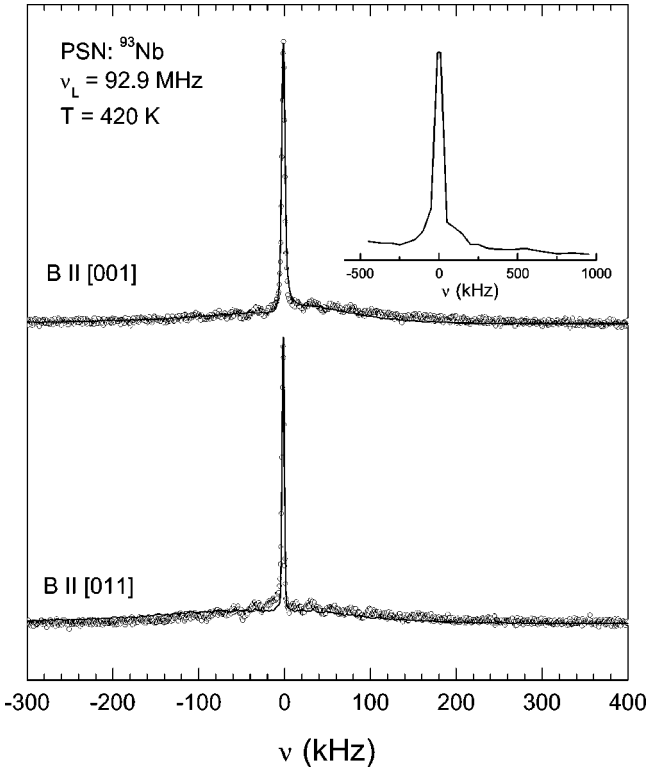

FIG. 2. ^{93}Nb NMR spectra in PSN. Points are experimental data; smooth lines correspond to calculated according to Eqs. (6)–(8) line shapes. The inset shows the ^{93}Nb spectrum measured by sweeping the irradiation frequency.

tween static and dynamic ion shifts. Some of our previous results devoted to NMR of relaxors have been published in Refs. 13 and 14.

The purpose of the present paper is to study the local structure of PMN and PSN at temperatures $T \gg T_m$ on the basis of ^{93}Nb and ^{45}Sc NMR measurements performed at a Larmor frequency $\nu_L \simeq 93$ MHz. The description of the NMR line shape was given on the basis of analytical formulas, allowing for both homogeneous and inhomogeneous mechanisms of line broadening. As a second approach, NMR spectra were analyzed using numerical Monte Carlo simulations and the point-charge point-dipole approximation for the electric-field gradients. The structural data obtained from the NMR are compared with similar data obtained from x-ray diffractions.

It should be noted that the present approach is different from the recently developed spherical random bond–random-field model,[15] which is mezoscopic and where information about the details of the local structure is lost.

II. SAMPLES AND EXPERIMENTAL DETAILS

The measurements were carried out on single-crystal samples of PMN and PSN grown on a seed crystal from the melt. Samples had a good optical quality. The sample dimensions of PSN were $(4\times4\times4)$ mm^3, and PMN—up to $(8\times8\times8)$ mm^3 with the surfaces parallel to crystallographic (001) planes. The degree of 1:1 Sc/Nb ordering in PSN varied in the range of 30–40 %. It was measured by using the superstructure (111) diffraction peaks associated to the Sc-Nb ordering along [111] direction.[16]

The NMR measurements were performed in a 9.2 T superconducting magnet at a ^{45}Sc Larmor frequency $\nu_L = 92.3$ MHz ($I=7/2$) and a ^{93}Nb $\nu_L = 92.9$ MHz ($I=9/2$). Temperature was stabilized in a continuous-flow cryostat with an accuracy of about 0.1 K. The inhomogeneously broadened spectra of ^{93}Nb and ^{45}Sc ($1/2 \leftrightarrow -1/2$ transition) have been obtained using the Fourier transform of the spin echo after a $(90_x - \tau) - (90_y - \tau)$–acquisition pulse sequence. The width of the 90° pulse was 2.1 μs and 2.4 μs for ^{93}Nb and ^{45}Sc resonances, respectively. The time delay τ was usually 40 μs for both nuclei.

III. EXPERIMENTAL RESULTS AND INTERPRETATION

A. ^{93}Nb and ^{45}Sc NMR spectra

Since we were mainly interested in the local structure of PMN and PSN in the high-temperature phase, i.e., at $T > T_m$, measurements were performed between 420–450 K. In Fig. 1 we present ^{45}Sc NMR spectra measured for three characteristic crystal orientations in the external magnetic field: $\mathbf{B}\|[001]$, [011], and [111] . The characteristic feature of the spectrum for $\mathbf{B}\|[001]$ and [111] is its strong asymmetry, while for $\mathbf{B}\|[011]$ the spectrum is almost symmetric. Similar spectra of ^{93}Nb in PSN and PMN are shown in Figs. 2 and 3, respectively. Note that in PMN, ^{93}Nb spectrum did not change either its shape or its width with increasing temperature up to 700 K, i.e., at $T > T_d$. Let us discuss first the Sc and Nb spectra in PSN.

Both the Sc and Nb spectra have an approximately similar structure and both contain a narrow component of the width of 3–4 kHz and a wide component that is different for the Sc and Nb nuclei. The narrow part of the spectra is well described by a Gaussian and is completely isotropic. On the contrary, the wide part is essentially anisotropic and cannot be precisely described by a simple function. In a rough approximation, however, it can be also described by a Gaussian (see Ref. 14). In such an approach, the ratio of the integral intensity of narrow and wide parts of the spectrum is $\approx 40{:}60$ and does not depend on the crystal orientation. Note that due to the large width of the ^{93}Nb spectrum, its wide component has a very small intensity and, thus, its anisotropy manifests itself much less than that in the ^{45}Sc spectrum. However, a measurement of the whole ^{93}Nb spectrum in PSN, using the sweep of the irradiation frequency, indeed showed that the Nb spectrum shape is very close to that of ^{45}Sc (inset to Fig. 2).

The ^{93}Nb spectrum in PMN is somewhat more complicated. In this spectrum we can conditionally separate three components: (1) a low-intensity isotropic line with the width of 3 kHz; (2) a spectrum around ν_L with a width of 15–18 kHz; (3) a wide and strong anisotropic component like that in PSN but more intensive. The narrow part with $\Delta\nu = 3$ kHz accounts only for about 2.5–3 % of the total integral intensity of the spectrum. As can be seen from Fig. 3, except for the narrowest component the whole spectrum is strongly anisotropic.

The anisotropy of the spectra as well as their asymmetric form with respect to ν_L for both ^{93}Nb and ^{45}Sc nuclei in PMN and PSN show that these spectra belong to the $1/2 \leftrightarrow -1/2$ transition, the frequency of which is shifted by the second-order quadrupolar contributions.[17] The very broad background spread symmetrically around the Larmor frequency is attributed to satellite transitions. Still another contribution comes from chemical shifts. The quadrupole contribution exists only for nuclei with a spin $I > 1/2$ and is related to the interaction of the nuclear quadrupole moment with the electric-field gradient (EFG). Large values of quadrupole moments of ^{93}Nb and ^{45}Sc nuclei ($eQ = -0.28e \times 10^{-28}$ m^2 and $-0.22e \times 10^{-28}$ m^2 for ^{93}Nb and ^{45}Sc, respectively) usually result in the predominance of the quadrupole contribution to NMR frequency shift with respect to other possible sources, such as chemical shift and magnetic dipole-dipole interaction. Therefore, we can conclude that the main features of ^{93}Nb and ^{45}Sc NMR spectra in both PMN and PSN are related to characteristic features of their EFG that depend on lattice ions charges and their positions, thus providing information on the local structure of crystals. Covalent contributions to the EFG are important too.

B. Analysis of ^{45}Sc and ^{93}Nb spectra in PSN and determination of the EFG tensors

The integral intensity ratio 40:60 obtained above for the narrow and wide parts of the ^{45}Sc and ^{93}Nb NMR spectra in PSN is in agreement with the Sc/Nb degree of ordering which varied in the studed crystals in the range of 30–40 %. So, it can be naturally assumed that narrow and wide parts of the spectra belong to the Sc and Nb nuclei situated in the ordered 1:1 and disordered regions of the crystal, respectively. Actually, in the ordered regions Sc and Nb ions are surrounded by a symmetrical ion configuration. Therefore, in such sites the electric-field gradients and anisotropic chemical shift must be close to zero and we can expect an NMR line broadened only by the magnetic dipole-dipole interaction. Calculation of this dipole-dipole width gives a value of about 3 kHz supporting the origin (ordered 1:1 regions) of narrow lines in ^{45}Sc and ^{93}Nb NMR spectra mentioned above.

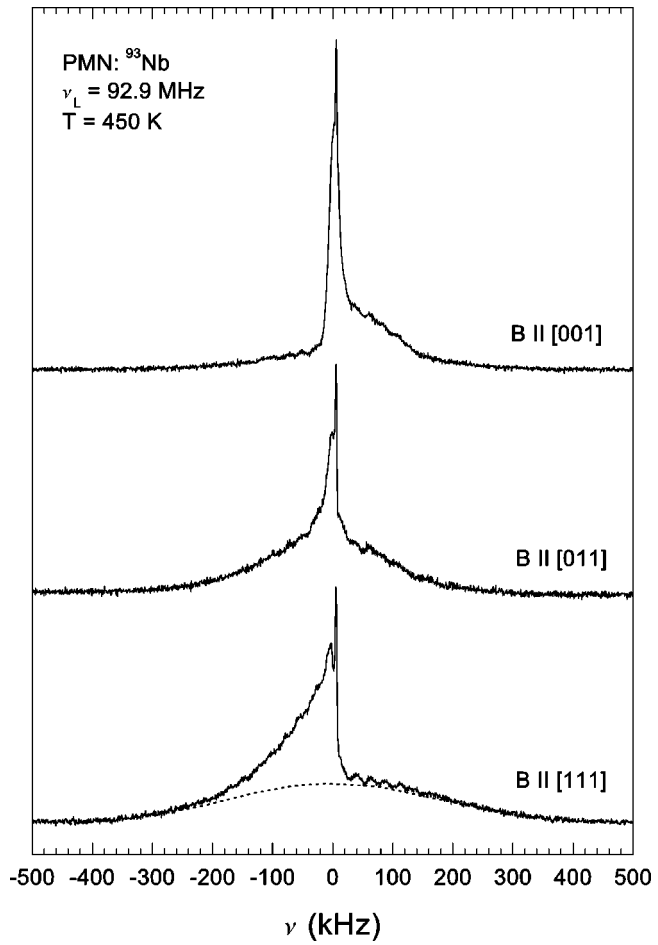

FIG. 3. ^{93}Nb NMR spectra in PMN. Dashed line shows unresolved quadrupole satellites.

The broad part of the the central transition NMR spectra belongs to resonances from nuclei located in the disordered regions of the crystal, where the random distribution of nonequally charged B'/B'' ions produces random electric-field gradients. Possible ionic shifts give an additional contribution to the EFG tensor components.

The second-order quadrupole shift of the $1/2 \leftrightarrow -1/2$ transition is proportional to the squared EFG. It can be written as

$$\nu = \alpha \nu_Q^2, \quad \alpha \equiv \frac{1}{6\nu_L}\left(I(I+1) - \frac{3}{4}\right) f_\eta(\theta, \varphi), \qquad (1)$$

where $\nu_Q = 3e^2qQ/2I(2I-1)h$, $eq = V_{zz}$, and $\eta = (V_{xx} - V_{yy})/V_{zz}$.

The function $f_\eta(\theta,\varphi)$ in Eq. (1) describes the dependence of the frequency shift on relative orientations of the external magnetic field and EFG tensor principal axes. ν_L is the Larmor frequency and x,y,z form the principal EFG tensor reference frame.

The angular variation of the broad part of the NMR spectra can be qualitatively understood if one assumes the presence of an axial EFG pointed at $\langle 001\rangle$ cubic directions. In this case, the angular part of expression (1) takes simple form

$$f(\theta,\varphi)=-\tfrac{3}{8}(1-\cos^2\theta)(9\cos^2\theta-1). \tag{2}$$

The expected resonances for all six $\langle 001\rangle$ directions of the EFG tensor are shown by histograms in Fig. 1. In our simple interpretation, we have to take into account that due to a large disorder in the ion positions, the EFG values become randomly distributed leading to a strong inhomogeneous broadening of NMR lines. As a result, only the shift of the center of gravity is visible in the experimental spectrum under crystal rotation. Due to the nonlinear relation between the resonance frequency shift and the quadrupole frequency, the inhomogeneously broadened NMR line acquires essentially the asymmetrical form, which depends on the orientation of the crystal in the external magnetic field. For such a complex spectrum, its decomposition into simple Gaussian components cannot give true values of quadrupole frequencies.

We introduce the distribution of the largest EFG component, which leads to the distribution of quadrupole frequencies ν_Q. Let us assume that the distribution function can be expressed in Gaussian form, i.e.,

$$F(\nu_Q)=\frac{1}{\sqrt{2\pi}\Delta}\exp\left(-\frac{(\nu_Q-\nu_Q^0)^2}{2\Delta^2}\right), \tag{3}$$

where ν_Q^0 is the mean value of the quadrupole frequency and Δ is the width of its distribution.

Allowing the nonlinear relation between ν and ν_Q [see Eq. (1)], the shape of the inhomogeneously broadened line can be written as (Ref. 18)

$$P(\nu)=\sum_{j=1}^{2}\frac{F(\nu_Q=\nu_{Qj})}{\left|\dfrac{d\nu}{d\nu_Q}\right|_{\nu_Q=\nu_{Qj}}},\qquad \nu_{Q_{1,2}}=\pm\sqrt{\frac{\nu}{\alpha}}. \tag{4}$$

Substitution of Eq. (1) into Eq. (4) gives

$$P(\nu)=\frac{1}{\sqrt{2\pi\alpha\nu}\Delta}\exp\left(-\frac{\nu+\alpha(\nu_Q^0)^2}{2\alpha\Delta^2}\right)\cosh\frac{\alpha}{\Delta^2}\sqrt{\frac{\nu}{\alpha}}. \tag{5}$$

To take into account the additional homogeneous broadening mechanism with a Gaussian lineshape one has to make the integration

$$I(\nu)=\frac{1}{\sqrt{2\pi}\delta}\int_{-\infty}^{\infty}P(\nu')\exp\left[\frac{-\ln 2(\nu-\nu')^2}{\delta^2}\right]d\nu', \tag{6}$$

with δ being a half of the Gaussian width.

One can see that Eqs. (5) and (6) give an asymmetrical line shape which depends also on the parameter $f(\theta,\varphi)$ that takes into account the mutual orientations of the EFG and the magnetic field $\mathbf{B}_0$.

One can expect that in disordered materials, there are microregions with different ''degree of order'' and different directions (and mean values) of the ion displacements. Obviously, in such a case the NMR line should be composed of the lines ''stemming'' from these microregions, i.e.,

$$I_q(\nu)=\sum_i I_{qi}(\nu), \tag{7}$$

where the subscript ''i''numerates the microregions.

The results of a simulation on the basis of Eqs. (5)–(7) of the ^{45}Sc NMR line shape for $\mathbf{B}\|[001]$ are presented by the solid line in Figs. 1(a) and 1(b). Figure 1(a) shows the line shape for the case of EFG with the largest principal axis pointing in $\langle 001\rangle$ directions only. The contribution from ordered regions, where $\nu_Q=0$ was also included. The best fit has been achieved for $|\nu_Q^0|=755$ kHz and $\Delta=210$ kHz. One can see that the calculated NMR line has a strongly asymmetrical shape, which fits very well the right ''shoulder'' of the measured spectrum. The fitting of left shoulder is not so good. This can be expected because for the $\langle 001\rangle$ orientation of the EFG, only a positive quadrupole shift of the resonance frequency exists [see Eqs. (1) and (2) when $\theta=90°;0°$]. Therefore, to fit the left shoulder of the observed spectrum, other orientations of EFG axes are required. The negative shift is possible for EFG axes pointing along $\langle 011\rangle$ and $\langle 111\rangle$ directions. The reason for this type of local distortions can be related to the substitutional disorder in the relaxors.

Finally, the experimental line shape of ^{45}Sc is well fitted by the following theoretical curve:

$$I_q(\nu)=C_0I_{ord}(\nu)+C_1I_{\langle 001\rangle}(\nu)+C_2I_{\langle 110\rangle}(\nu)+C_3I_{\langle 111\rangle}(\nu) \tag{8}$$

with $C_0\simeq 0.3, C_1\simeq 0.45, C_2\simeq 0.11, C_3\simeq 0.14$; the subscripts denote the direction of the EFG axes. The result of a complete ^{45}Sc spectrum simulation is presented in Fig. 1(b).

The obtained set of fitting parameters (all of them are presented in Table I) permits to describe theoretically the NMR line shapes measured for any other orientation of magnetic field. In particular, in Figs. 1(c) and 1(d), the observed and calculated line shapes for $\mathbf{B}\|[011]$ and $\mathbf{B}\|[111]$ are shown.

Similar simulations performed for the ^{93}Nb NMR spectra are presented in Fig. 2 by solid lines and the corresponding fitting parameters are listed in Table I. The agreement between measured and calculated spectra is good. However, due to small intensity of the broad part of the spectrum, the obtained parameters contain significantly bigger errors than for the ^{45}Sc spectra.

C. Analysis of ^{93}Nb NMR spectra in PMN

It can be seen from Fig. 3 that practically the whole ^{93}Nb spectrum in PMN is strongly broadened in comparison with

TABLE I. ^{45}Sc and ^{93}Nb NMR parameters determined in disordered PSN and PMN at $T=450$ K.

Compound	(e^2qQ/h) (MHz)	Distribution Δ (MHz)	Homogeneous width (kHz)	$\lvert V_{zz}\rvert(10^{20}$ V m$^{-2})$	Orientation of V_{zz}
$PbSc_{1/2}Nb_{1/2}O_3$					
^{45}Sc	10.6(5)	2.9(4)	4	20(1)	$\langle 001\rangle$
	9(1)	4.9(5)		17(2)	$\langle 011\rangle$
	8.8(10)	4.9(5)		16(2)	$\langle 111\rangle$
^{93}Nb	46(3)	15(2)	8	68(5)	$\langle 001\rangle$
	42(6)	20(4)		62(8)	$\langle 011\rangle$
	56(6)	27(4)		83(10)	$\langle 111\rangle$
$PbMg_{1/3}Nb_{2/3}O_3$					
^{93}Nb	46(3)	24(3)	18	68(5)	$\langle 001\rangle$
	60(3)	29(3)		89(6)	$\langle 011\rangle$
	36(3)	29(3)		53(5)	$\langle 111\rangle$

the dipole-dipole width that is equal to 2.8–3.6 kHz (as in the case of PSN). The portion of the spectrum unbroadened by the quadrupole mechanism or by an anisotropic chemical shift accounts only for 2–3 % of the total intensity. It is clear that the Nb nuclei, which contribute to this narrow spectrum, are located at positions close to the regular cubic ones. The broad main part of the ^{93}Nb spectrum is related to the disordered, locally noncubic, regions of the crystal.

The ^{93}Nb spectrum for PMN was fitted assuming local distortions along $\langle 001\rangle$, $\langle 110\rangle$, or $\langle 111\rangle$ directions, i.e., as in the case of the PSN by Eq. (8). Since the procedure of the simulation is similar to that described for PSN, we here presented in Table I only the spectral parameters derived. Comparing spectral data for disordered PSN and PMN one can emphasize a similarity in the symmetry and sometimes even in the values of electric-field gradients at Nb positions. However, the homogeneous width of 18 kHz obtained in PMN is much larger than that expected for the ^{93}Nb dipole-dipole width. A reason for this will be discussed in the following section. One can also see that the distribution of EFG in PMN is larger than in PSN. This is in agreement with the fact that in PMN local lattice distortions should be much larger due to bigger differences in the ionic charges of B' and B'' cations.

D. Numerical calculation of the EFG tensor and NMR line shape

In the preceding section, the mean values of quadrupole coupling constants at the Sc and Nb cation positions as well as their dispersions were obtained on the basis of an analytical calculation of the shape of the inhomogeneously broadened NMR line. The method has allowed to take into account only the distribution of the quadrupole frequencies ν_Q, but the presence of random deviations of EFG axes from their most probable directions, i.e., the fluctuation of $f_\eta(\theta,\varphi)$ [see Eq. (1)] was not taken into account to obtaine simple analytical formulas. Ignoring these fluctuations has resulted in much too high values of the homogeneous width, 4 kHz and 8 kHz for the ^{45}Sc and ^{93}Nb in PSN and 18 kHz for the ^{93}Nb in PMN.

The second reason to undertake numerical calculation of NMR line shape and EFG is related to the attempt to determine main sources of the EFG in both relaxor systems. In view of the complexity and substantial uncertainty of the local structure of these compounds, we used the simple point-charge point-dipole model. However, we also took into account effects related to partial covalency of bonds in the BO_6 octahedron as well as an electronic polarization to overcome the restrictions of point-charge model.

In the point-charge point-dipole approximation, the electric-field-gradient components at the site of the nucleus are given by

$$V_{ij}=(1-\gamma_\infty)\sum_k \frac{\partial^2}{\partial x_i \partial x_j}\left[\frac{q_k}{r_k}+\frac{r_{ik}\mu_{ik}}{r_k^3}\right], \tag{9}$$

where q_k and μ_k are the electric point charge and dipole moment of the kth ion, respectively, r_k is the distance between the kth ion and the observation point, and $1-\gamma_\infty$ is the antishielding parameter. For ^{93}Nb the parameter $1-\gamma_\infty=16$ was taken as in other ABO_3 crystals such as $KNbO_3$.[19] For the ^{45}Sc ion, the antishielding parameter is rather uncertain. However, clearly its value has to be smaller in comparison with ^{93}Nb due to smaller number of electronic orbitals. The value $1-\gamma_\infty=9$ leads to the best agreement with the experimental spectrum.

Three different contributions to the EFG were considered in the sum (9). The first contribution $V_{ij}^{(1)}$ is related to the random distribution of charges of B'/B'' ions at lattice points of the ideal $AB\,O_3$ perovskite structure. Contributions of ions at a distance up to five lattice constants (2 nm) were summed up. However, usually the distance up to 1.2–1.5 nm was sufficient due to the rapid decay of V_{ij} with the distance. In the calculations, the B-type ions were randomly distributed at lattice sites or they were located in the 1:1 or 1:2 ordered regions. The main condition for any ion configuration was electroneutrality, i.e., the stoichiometric (in average 1:1 for PSN and 1:2 for PMN) composition in the calculated region was conserved.

As an example, the result of the calculation of the largest component V_{zz} as a function of polar angle θ for PMN is

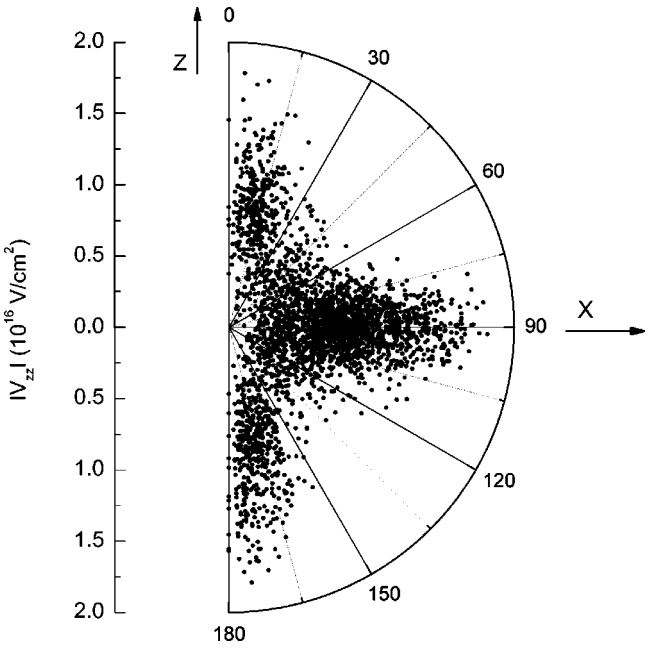

FIG. 4. Polar plot of the $|V_{zz}|$ EFG component at Nb sites in PMN calculated for random distributions Mg^{2+} and Nb^{5+} at lattice points of the ideal ABO_3 structure.

presented in Fig. 4. Here, we took the effective valence charges of Mg^{2+} and Nb^{5+} as one-half of their formal charges. It is seen that V_{zz} lies close or along cubic directions, but is strongly distributed in both the magnitude and orientation. The mean value $|\overline{V_{zz}}|=0.78\times10^{16}$ V/cm^2 ($e^2qQ/h\simeq15$ MHz) is much less than that expected from the coupling constant measured. Thus, this contribution to the EFG cannot be responsible for the wide component of the ^{93}Nb NMR line. It can give only some contribution to homogeneous broadening of NMR line because it leads to a distribution of directions of principal axes of the total EFG. Note that in $PbSc_{1/2}Nb_{1/2}O_3$, this part of EFG is small in comparison even with the dipole-dipole width due to the smaller difference between charges of Sc^{3+} and Nb^{5+} and, in addition, 1:1 type relaxors have a more symmetrical distribution of B'/B'' ions.

The second contribution $V_{ij}^{(2)}$ to the EFG accounts for the shifts of B'/B'' ions themselves relatively to the nearest six oxygen ions. Possible shifts of Pb^{2+} ions were not taken into account due to their smaller (10–15 times) contribution to the EFG for the same values of the shifts. In a general case for an arbitrary *B*-type ion shift with respect to the center of the undistorted oxygen octahedron, the following expressions for the EFG tensor components were obtained:

$$V_{ii}^{(2)}=(1-\gamma_\infty)\frac{21z_O^{val}}{b^5}(3d_i^2-d^2),$$

$$V_{ij}^{(2)}=-(1-\gamma_\infty)\frac{42z_O^{val}}{b^5}d_id_j,\quad i\neq j, \tag{10}$$

where (d_x, d_y, d_z) are vector components of the Nb or Sc shift, z_O^{val} is the effective valence charge of the oxygen, and $b=a/2$ (a is the lattice constant). For simplicity, the z_O^{val} was taken as an average value over all six oxygen ions. Its value may lay in the range between $-1.63|e|$($BaTiO_3$) (Ref. 20) and $-0.85|e|$ ($KNbO_3$).[21]

The last term in Eq. (9) is related to the induced electric dipole moments μ_i. Assuming that only the electronic polarization of the nearest six oxygenions gives a marked contribution to the EFG (the other ions in the unit cell and the next-nearest oxygens give contributions that are an order of magnitude smaller), the dipole contibution is

$$V_{zz}=(1-\gamma_\infty)\frac{84\mu}{b^5}d,\quad V_{xx}=V_{yy}=-V_{zz}/2,$$

$$V_{ij}=-(1-\gamma_\infty)\frac{84\mu_i}{b^5}d_j,\quad i\neq j, \tag{11}$$

where μ is assumed to be in the direction of the Z axis of the field gradient.

The electronic dipole moment is usually calculated from a knowledge of the polarization and the internal electric field. For disordered relaxors, this is not suitable because only a local polarization exists and there is a large uncertainty in the ion positions. Therefore, for the calculation of V_{ij} we applied the method of effective dipole moments, where electronic dipole moment can be expressed as $\mu_i=Z_O^*d_i$, and Z_O^* is the Born effective charge of oxygen. Taking into account the special role of Pb ions, namely, their strong hybridization with oxygen ions, we used the effective charges derived in $PbTiO_3$ where they successfully describe the spontaneous polarization.[22] For simplicity, the same avarage value of $Z_O^*=-4|e|$ was taken for six oxygenions in the octahedron. One can see that under these conditions, expressions (10) and (11) become similar but with predominance of electronic part because $Z_O^*\gg Z_O^{val}$. Note that similar results were obtained in $KNbO_3$ (Ref. 19) and $BaTiO_3$.[23]

Taking into account that the ion shifts have random values due to the disorder of the Mg, Nb, and Sc positions, the ion shift distribution function was assumed in the Gaussian form

$$f(d)=\frac{1}{\sigma(2\pi)^{1/2}}\exp\left(-\frac{(d-d_0)^2}{2\sigma^2}\right), \tag{12}$$

where d_0 is the mean value of the shift and σ is its dispersion.

The NMR spectrum intensity $I(\nu)$ was obtained by summing the contributions of the NMR lines from a large number of clusters (usually, 15 000–20 000), in which the *B*-type ions could be shifted in one of the three directions: $\langle001\rangle$, $\langle011\rangle$, or $\langle111\rangle$.

As an example, the results of ^{45}Sc spectrum calculation in PSN and ^{93}Nb spectrum calculation in PMN for $\mathbf{B}\|[001]$ are presented in Figs. 5(a) and 5(b), respectively. The individual contributions that are related to the Sc and Nb shifts in different directions with respect to oxygen positions are presented in the figures as well. Corresponding values of ion

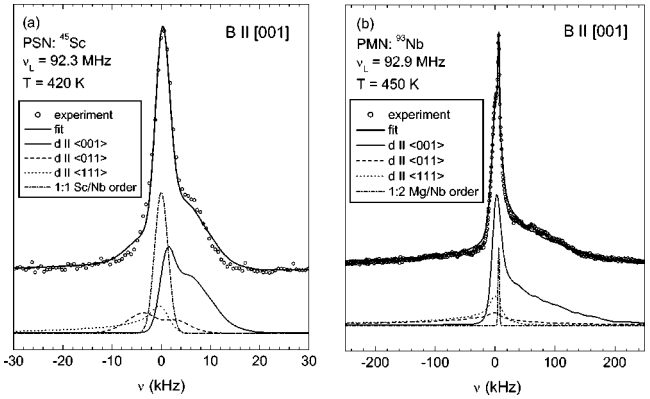

FIG. 5. Comparison between calculated on the base of Eqs. (9)–(12) and measured ^{45}Sc NMR spectrum in PSN (a) and ^{93}Nb NMR spectrum in PMN (b) at orientation $\mathbf{B}\|[001]$. Separate contributions to the NMR spectrum connected with different type of ion shifts are shown in the bottom panels by solid line ($d\|\langle 001\rangle$), dashed line ($d\|\langle 011\rangle$), and dotted line ($d\|\langle 111\rangle$); contributions from 1:1 Sc/Nb and 1:2 Mg/Nb ordered regions are shown by the dash-dot lines.

shifts and their distribution are given in Tables II and III. Obtained data clearly show that the dipole moments of off-center shifted lattice ions are the main source of large EFG in PMN and disordered PSN. As it follows from Fig. 5(b) such local noncubic regions occupy practically whole volume of the PMN crystal. In these noncubic regions, lattice ions are randomly shifted away from their cubic lattice sites in one of the directions: $\langle 001\rangle$, $\langle 011\rangle$, or $\langle 111\rangle$. The larger part of ions ($\sim$50%) experiences a shift along $\langle 001\rangle$ axes. On the contrary, in the ordered regions the Sc^{3+}, Nb^{5+}, and O^{2-} ions occupy completely cubic lattice positions, i.e., they are not shifted.

However, the following two comments should be made.

(i) The values presented in Tables II and III are the relative shifts between Nb(Sc) and oxygen ions, i.e., $d_{Nb(Sc)-O}$. A larger contribution to $d_{Nb(Sc)-O}$ values due to oxygen-ion shift rather than that of Nb(Sc) ions is expected in accordance with x-ray data.[4]

(ii) The real values of ion shifts can be somewhat different from those given in Tables II and III due to simplifications made in the calculations, including the point-charge model. However, the conclusion about the existence of the displacements, their directions and distribution is not related to the model of EFG calculation because they follow directly from the observed shape and width of ^{45}Sc and ^{93}Nb NMR lines.

TABLE II. Parameters of ionic shifts in PSN at $T=420$ K derived from NMR data. Estimated error bar of ionic shifts is 25–30 %.

		Direction of ions shifts		
	1:1 Ordered	$\langle 001\rangle$	$\langle 011\rangle$	$\langle 111\rangle$
Portion (%)	30	35	15	20
$d_{Sc\text{-}O}$ nm)	0	0.015	0.016	0.017
Distribution σ (nm)	0	0.001	0.001	0.001
$d_{Nb\text{-}O}$ (nm)	0	0.016	0.018	0.022
Distribution σ (nm)	0	0.005	0.005	0.005

TABLE III. Parameters of ionic shifts in PMN at $T=450$ K derived from NMR data. Estimated error bar of ionic shifts is 25–30 %.

		Direction of ions shifts		
	1:2 Ordered	$\langle 001\rangle$	$\langle 011\rangle$	$\langle 111\rangle$
Portion (%)	2	56	21	21
$d_{Nb\text{-}O}$ (nm)	0	0.016	0.021	0.017
Distribution σ (nm)	0	0.005	0.01	0.01

IV. DISCUSSION

The key to understanding the origin of unusual physical properties of relaxor ferroelectrics is their local structure. At any temperature and even on a micrometric scale, the average symmetry of PMN, for instance, is cubic rather than a lower one (see, for instance, Refs. 3 and 24). In contrast to PMN, PSN at $T<T_C$ ($T_C\approx 350$–360 K) undergoes a transition into the $R3m$ rhombohedral ferroelectric phase.[4,25] Note that the polar long-range order appears not only in perfect 1:1 Sc/Nb ordered PSN, but even in partially ordered crystals.[4] The compositional disorder thus does not prevent the establishing of long-range order. This may correspond to a mixed ferroglass phase. It is important to compare the local structures of PSN and PMN on the basis of NMR data because many of the new models, which describe the behavior of PMN at low temperatures, are based on the existence of 1:1 Mg/Nb ordered microregions similar to 1:1 Sc/Nb regions in PSN.

It is clearly seen from Figs. 1 and 2 that for 1:1 ordered regions in PSN a distinct narrow lines in both ^{45}Sc and ^{93}Nb NMR spectra are obtained. In these regions, Sc and Nb ions are located in regular cubic lattice sites, where the total electric-field gradient is zero or close to zero. The ^{93}Nb NMR spectrum in PMN also exhibits a narrow component (Figs. 3 and 5) but its integral intensity is only about 2.5–3 % of the total spectrum intensity (Table III). Evidently, this is the reason to ascribe this ^{93}Nb resonance to the regular 1:2 Mg/Nb ordered regions of the crystal. Note that this resonance could not belong to 1:1 Mg/Nb ordered regions because in agreement with high-resolution electron microscopy study[26] the portion of such ordered regions (if they exist) should be $\approx$30%. Thus, if local ($\sim$1.5–2.5 nm) 1:1 ordered clusters exist in PMN, the disagreement between NMR and electron microscopy data can be overcome only by assuming that in these local regions the niobium and oxygen ions are off-center shifted as in completely disordered regions. This fact seems to be strange. Let us remind that the Sc and Nb ions in 1:1 Sc/Nb ordered PSN are situated in correct cubic lattice sites. Taking into account this argument, the model based on the alternation of Nb and ($Mg_{2/3}Nb_{1/3}$) layers which also explains the observation of $1/2\langle 111\rangle$ superlattice diffraction peak[12,27,28] seems to be more convincing. In this model local strains induced by the charge disbalance between the Nb and Mg/Nb layers can be locally compensated

by oxygen-ion displacements which will give a contribution to the electric-field gradient. Additional contributions to EFG are also due to ($Mg_{2/3}Nb_{1/3}$) layer compositional disorder.

It is important to emphasize that our data relating to the noncubic local structure of PMN clearly demonstrate that we cannot describe the relaxor state in PMN as consisting of static polar nanoregions embedded in a nonpolar cubic matrix as it was assumed in Ref. 10 because even on the NMR time scale (10^{-5}–10^{-8} s) the cubic symmetry is locally broken practically in whole crystal volume. Consequently, the relaxor state in PMN has to be considered as polar nanoregions embedded in a nonpolar noncubic matrix.

The above results by themselves cannot exclude the possibility that ion shifts in one out of three observed directions may be the result of a ferroelectric phase transition at the Burn's temperature $T_d = 640$ K. A recent neutron inelastic-scattering measurement of the lowest-energy TO phonon branch in PMN really have shown that above T_d zone center, TO mode softens in a manner consistent with that of a ferroelectric soft mode.[9] Below T_d, the soft mode is overdamped by randomly oriented polar nanoregions which arise at T_d. Obviously, the noncubic local structure of PMN has to be accounted for the temperature behavior of the soft TO mode as well. According to a model proposed by some of us several years ago,[29] strong random fields existing in noncubic structure completely destroy the ferroelectric long-range order that could be established at $T < T_d$ because the correlation radius r_c decreases at $T < T_d$ (here, r_c is the correlation radius of the lattice that should be responsible for the phase transition at T_d). As a result only small movable polar clusters would appear below T_d. In such a picture, the strong dispersion and *V-F* law, observed in the temperature dependence of dielectric permitivity in PMN (see, e.g., Ref. 30, and reference therein) can be considered as a manifestation of the reentrant of the Burn's reference phase (like that in magnetic systems).[31]

Note that no anomalous T dependence of the Nb NMR line shape has been observed by us at Burn's temperature, but this cannot speak against the possibillity that a ferroelectric transition occurs at T_d because, for example, in PSN ^{93}Nb, NMR spectrum does not show any anomaly at the temperature of phase transition as well.[32] On the contrary, ^{207}Pb NMR spectrum changes drastically in PSN at $T < T_C$. Thus, further studies, especially ^{207}Pb NMR spectra, are necessary to clear up all a forementioned questions.

[1] G.A. Smolenskii and V.A. Isupov, Dokl. Akad. Nauk SSSR **97**, 653 (1954).

[2] L.E. Cross, Ferroelectrics **76**, 241 (1987).

[3] P. Bonneau, P. Garnier, G. Calvarin, E. Husson, J.R. Gavarri, A.W. Hewat, and A. Morell, J. Solid State Chem. **91**, 350 (1991).

[4] C. Malibert, B. Dkhil, J.M. Kiat, D. Durand, J.F. Berar, and A. Spasojevic-de Bire, J. Phys.: Condens. Matter **9**, 7485 (1997).

[5] P. Bonneau, P. Garnier, E. Husson, and A. Morell, Mater. Res. Bull. **24**, 201 (1989).

[6] S. Vakhrushev, S. Zhukov, G. Fetisov, and V. Chernyshov, J. Phys.: Condens. Matter **6**, 4021 (1994).

[7] G. Burns and F.H. Dacol, Solid State Commun. **13**, 423 (1973); Phys. Rev. B **28**, 2527 (1988).

[8] A. Naberezhnov, S. Vakhrushev, B. Dorner, D. Stranch, and H. Moudden, Eur. Phys. J. B **11**, 13 (1999).

[9] P.M. Gehring, S. Wakimoto, Z.-G. Ye, and G. Shirane, Phys. Rev. Lett. **87**, 277601 (2001).

[10] K. Hirota, Z.-G. Ye, S. Wakimoto, P.M. Gehring, and G. Shirane, Phys. Rev. B **65**, 104105 (2002).

[11] P.K. Davies and M.A. Akbas, J. Phys. Chem. Solids **61**, 159 (2000).

[12] Y. Yan, S.J. Pennycook, Z. Xu, and D. Viehland, Appl. Phys. Lett. **72**, 3145 (1998).

[13] M.D. Glinchuk, V.V. Laguta, I.P. Bykov, S. Nokhrin, V.P. Bovtun, M.A. Leschenko, J. Rosa, and L. Jastrabik, J. Appl. Phys. **81**, 3561 (1997).

[14] R. Blinc, A.A. Gregorovič, B. Zalar, R. Pirc, V.V. Laguta, and M.D. Glinchuk, J. Appl. Phys. **89**, 1349 (2001).

[15] R. Blinc, J. Dolinšek, A. Gregorovič, B. Zalar, C. Filipič, Z. Kutnjak, A. Levstik, and R. Pirc, Phys. Rev. Lett. **83**, 424 (1999).

[16] C.G.F. Stenger and A.J. Burggraaf, Phys. Status Solidi A **61**, 275 (1980).

[17] A. Abragam, *The Principles of Nuclear Magnetism* (Clarendon, Oxford, 1961).

[18] M.D. Glinchuk and I.V. Kondakova, Sov. Sol. St. Phys. **40**, 340 (1998).

[19] R.R. Hewitt, Phys. Rev. **121**, 45 (1961).

[20] R.E. Cohen and H. Krakauer, Phys. Rev. B **42**, 6416 (1990).

[21] R.I. Eglitis, A.V. Postnikov, and G. Borstel, Phys. Rev. B **54**, 2421 (1996).

[22] U.V. Waghmare and K.M. Rabe, Phys. Rev. B **55**, 6161 (1997).

[23] A.S. Viskov and Yu.N. Venevcev, Fiz. Tverd. Tela (St. Peterburg) **8**, 416 (1966).

[24] N. -de Mathan, E. Husson, G. Calvarin, J.R. Gavarri, A.W. Hewat, and A. Morell, J. Phys.: Condens. Matter **3**, 8159 (1991).

[25] K.S. Knight and K.Z. Baba-Kishi, Ferroelectrics **173**, 341 (1995).

[26] C. Boulesteix, F. Varnier, A. Llebaria, and E. Husson, J. Solid State Chem. **108**, 141 (1994).

[27] T. Egami, W. Dmowski, S. Teslic, P.K. Davies, I.-W. Chen, and H. Chen, Ferroelectrics **206-207**, 231 (1998).

[28] J. Chen, H.M. Chan, and M.P. Harmer, J. Am. Ceram. Soc. **72**, 593 (1989).

[29] M.D. Glinchuk and R. Farhi, J. Phys.: Condens. Matter **8**, 6985 (1996).

[30] M.D. Glinchuk and V.A. Stephanovich, J. Appl. Phys. **85**, 1722 (1999).

[31] J.Ya. Korenblit and E.F. Shender, Usp. Fiz. Nauk **157**, 267 (1989).

[32] V.V. Laguta, M.D. Glinchuk, I.P. Bykov, R. Blinc, and B. Zalar, in *Proceedings of the Second Open Franco-Ukraine Workshop on Ferroelectricity, Dinard, France, 2002*, edited by A. Perrin (University of Rennes, Rennes, 2002), p. 7.